Characterizing Polymer-Grafted Nanoparticles: From Basic Defining Parameters to

**Behavior in Solvents and Self-Assembled Structures** 

Andrew J. Chancellor, Bryan T. Seymour, and Bin Zhao\*

Department of Chemistry, University of Tennessee, Knoxville, Tennessee 37996, United States

Corresponding author. Email: <u>bzhao@utk.edu</u> (B.Z.). Phone: 1-(865)974-3399

Abstract

Polymer-grafted nanoparticles, often called hairy nanoparticles (HNPs), are an intriguing class of

nanostructured hybrid materials with great potential in a variety of applications, including

advanced polymer nanocomposite fabrication, drug delivery, imaging, and lubrication. This

Feature Article provides an introduction to characterization of various aspects of HNPs, from basic

defining parameters to behavior of HNPs in solvents and self-assembled structures of

multicomponent brush nanoparticles, by using a broad range of analytical tools.

1

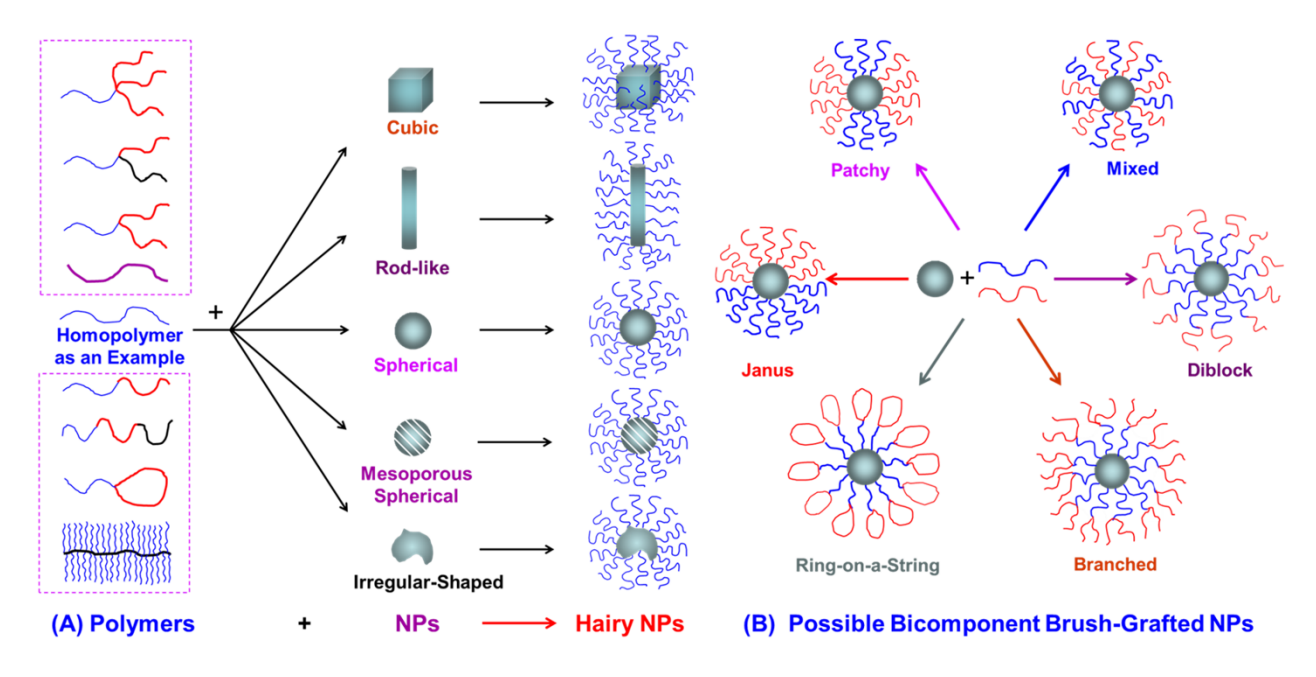
#### Introduction

Polymer-grafted nanoparticles (NPs), also called hairy NPs (HNPs), are an intriguing class of nanostructured materials consisting of a layer of macromolecular chains covalently grafted on the surface of NPs, often inorganic and metallic.<sup>1-4</sup> Capable of exhibiting unique, combined properties of core NPs and surface-tethered polymers, HNPs have received tremendous interest in the past two decades and have shown great promise in a variety of applications, including advanced polymer nanocomposite fabrication, drug delivery, sensing, imaging, aqueous and oil lubrication, and catalysis.<sup>1-12</sup> HNPs feature numerous design possibilities of combining polymers and NPs (Scheme 1). The core can be solid, mesoporous, or hollow, with a size ranging from a few to hundreds of nanometers. 12-16 In terms of geometry, the core NPs could have a regular shape, such as spherical, cubic, and rod-like, or an irregular shape. 11-19 Compositionally, although the core NPs are often inorganic and metallic, polymers have also been employed.<sup>20,21</sup> On the other hand, the surface-grafted polymers can have various chemical compositions and topologies, such as homopolymers, random copolymers, block and star copolymers, bottlebrushes, and cyclic polymers, as well as different grafting densities; possible examples of bicomponent polymer brushgrafted NPs are schematically illustrated in Scheme 1B.9,22-29 Imaginably, each combination represents a set of HNPs with unique structures and potentially interesting behavior. Despite vast possibilities of combining polymers and NPs to form HNPs, so far only a very limited set of welldefined HNPs has been synthesized and experimentally studied due to the challenges in synthesis and characterization.

Inorganic and metallic NPs have been shown to exhibit fascinating optical, magnetic, catalytic, mechanical, and lubricating properties, many of which are associated with size-related quantum effects.<sup>30-33</sup> However, processing these NPs after the synthesis remains a big challenge because of

the high tendency of NPs to undergo aggregation. As a matter of fact, many as-synthesized NPs, once fully dried, cannot be re-dispersed as individual NPs in any solvents. Grafting polymer chains on NPs has proven to be an effective means to improve the processability of NPs. The superior dispersibility and stability of high grafting density HNPs in solvents, as demonstrated by many researchers, originate from the favorable enthalpic interactions between the grafted polymer and the solvent and the entropic repulsive interactions between HNPs. Similarly, HNPs can be more readily blended into a polymer matrix of the same type to form nanocomposites, particularly when the molecular weight of the polymer matrix is smaller than that of the grafted polymer. 5-7,35

**Scheme 1.** (A) Schematic Illustration of Various Types of Polymer-Grafted Nanoparticles by Combining Polymers with Different Architectures and NPs Using a Homopolymer as an Example and (B) Examples of Bicomponent Brush NPs



If the grafted polymers are stimuli-responsive, that is, the polymers undergo relatively large conformational and solubility changes in response to small environmental variations such as temperature and pH,<sup>36-39</sup> the HNPs' behavior can be controlled by external stimuli. These

responsive HNPs have been shown to exhibit intriguing behaviors, such as reversible aggregation/dispersion, reversible phase transfer between immiscible liquid phases, tunable catalytic activity, triggered drug release, reversible color changes, etc., testifying to how the grafted polymer dictates the interactions of HNPs with each other and the environment. 19,40-47

From the standpoint of polymer science, the phase behavior of multicomponent brushes in a confined geometry is an interesting topic. 48,49 However, it is very challenging to apply commonly used analytical tools for studying block copolymers, such as transmission electron microscopy (TEM) and small angle X-ray scattering, to characterize multicomponent brushes on flat substrates. In contrast, when silica NPs are used as substrates, one can directly use TEM and other means to study the morphology of brushes on NPs.<sup>2</sup> On the other hand, non-planar substrates introduce a new parameter, curvature, to the brush system, whose effect on the morphology of multicomponent brushes is largely unknown, although it has been studied theoretically but rarely experimentally. 49,50

Characterization is crucial for synthesizing HNPs with prescribed molecular parameters, elucidating their structures, understanding their behavior and properties, and using them in specific applications. The structures, behavior, and properties of HNPs are fundamentally governed by basic parameters such as molecular weights, dispersity, grafting density, polymer topology, size and geometry of core NPs, etc. Accurate characterization of basic defining parameters and other aspects of HNPs requires the use of a broad range of characterization techniques. This Feature Article is intended to serve as an introduction to characterization of HNPs. As mentioned earlier, HNPs are a highly versatile class of hybrid materials with potential applications in many different areas. While specific applications of hairy NPs may involve the use of special analytical tools, we focus in this Article on: (1) determining basic defining parameters of HNPs, (2) probing their

behavior in solvents, and (3) elucidating self-assembled structures of multicomponent brush NPs after a discussion on HNP synthesis. The first two are fundamental for virtually all uses of HNPs, while the third one has attracted considerable interest in recent years. Table 1 lists the more detailed aspects of HNPs to be discussed and the corresponding characterization tools. The principles of characterization techniques will be briefly introduced, and the challenges in the study of complex HNPs will be discussed.

**Table 1.** Aspects of HNPs Discussed in this Article and Corresponding Characterization Techniques

Aspects of Hairy NPs	Characterization Techniques *
1. Basic Defining Parameters	
Molecular Weight, Dispersity (D)), and Degree of	SEC, NMR, TGA
Polymerization (DP) of Grafted Polymer	
Chemical Composition of Grafted Polymer	NMR, TGA
Grafting Density of Grafted Polymer	SEC, NMR, TGA, TEM
Characteristics of Core NPs	TEM, Nitrogen Adsorption-
	Desorption (BET Method)
2. Behavior in Solvents	Visual Inspection, DLS, TEM
3. Self-Assembled Structures of Multicomponent Brushes	SEM, TEM, Cryo-TEM, TEM-ET

<sup>\*</sup> SEC: size exclusion chromatography; NMR: nuclear magnetic resonance; TGA: thermogravimetric analysis; TEM: transmission electron microscopy; BET method: Brunauer–Emmett–Teller method; DLS: dynamic light scattering; Cryo-TEM: cryogenic transmission electron microscopy; TEM-ET: transmission electron microscopy – electron tomography

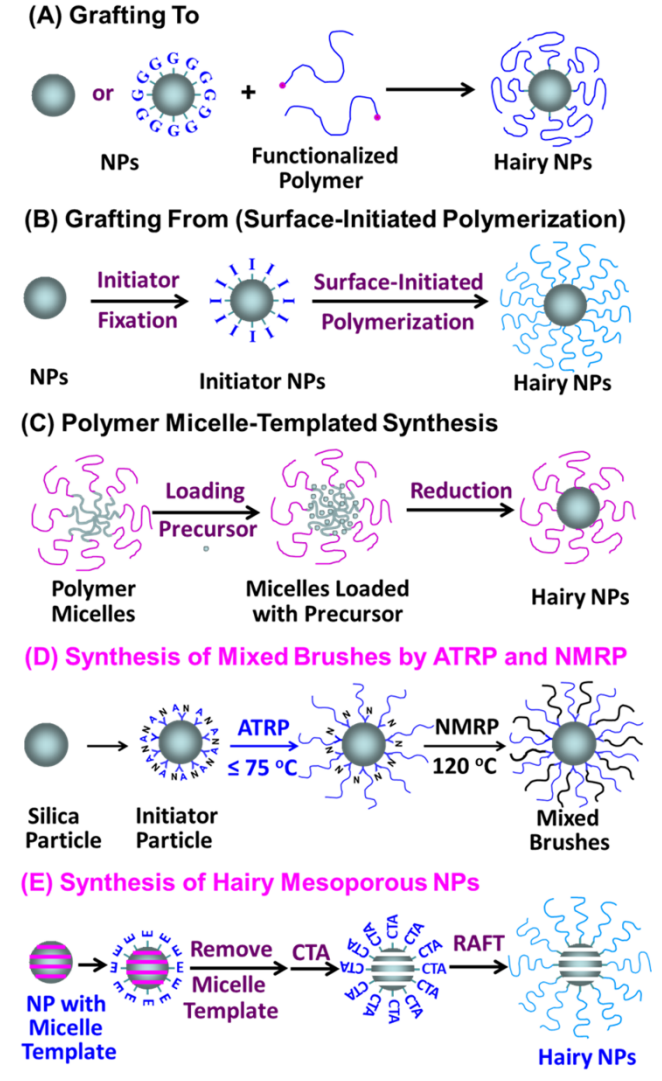
# **Synthesis of HNPs**

HNPs are commonly prepared by three methods or their combinations for more complex systems (Scheme 2): (i) grafting to, where a functionalized polymer reacts with the surface or complementary groups on the surface of NPs, (ii) grafting from, where an initiator is fixed on NPs following by surface-initiated polymerization to grow polymer chains, and (iii) templated synthesis, where multimolecular or unimolecular polymer micelles are loaded with a precursor, which is subsequently converted to NPs with the outer block serving as grafted chains.<sup>1-29,40-47,51</sup>-

- (i) "Grafting to". Methodologically, "grafting to" is the most straightforward among the three methods (Scheme 2A), where functional groups, such as thiol or carboxylic acid, incorporated at the end or in the middle of polymer chains react directly with NPs (e.g., gold NPs) or with complementary chemical groups (e.g., hydroxyl or epoxy) on the surface of NPs, resulting in the grafting of polymer chains on NPs. 19,51-56 This method can be used to synthesize simple HNPs such as homopolymer or random copolymer-grafted NPs as well as binary polymer-grafted NPs. For example, binary mixed brush-grafted Au NPs have been prepared by this method, either directly using two chemically distinct thiol or (di or tri)thiocarbonate end-functionalized polymers as stabilizing ligands in the synthesis of gold NPs or grafting them onto Au NPs, which allows for facile tuning of the molar ratio of two polymer ligands on NPs. 51-53 One main advantage of "grafting to" is that the polymers and NPs can be thoroughly characterized before the reaction. However, the polymer grafting density ( $\sigma$ ), defined as the number of end-tethered polymer chains per unit surface area of NPs (chains/nm<sup>2</sup>), tends to be low due to the steric hindrance presented by the already grafted chains to the incoming molecules. In addition, the polymer-metal bonding may be weak (e.g., S-Au bond), and de-grafting could occur.
- (ii) "Grafting from". Over the past two decades, "grafting from" (Scheme 2B) in conjunction with "living"/controlled polymerization has emerged as a robust, versatile method for the synthesis of well-defined HNPs with high grafting densities, controlled molecular weights, narrow dispersities, and well-defined architectures. 1-4,10-15,40-44,46,47,58-60 The commonly used "living" polymerization techniques include various forms of atom transfer radical polymerization (ATRP), nitroxide-mediated radical polymerization (NMRP), and reversible addition-fragmentation chain transfer (RAFT) polymerization. An initiator or a RAFT chain transfer agent (CTA) is immobilized onto the surface of NPs, followed by surface-initiated polymerization to grow

polymer chains from the NP's surface. Under the optimized conditions, grafting densities in the range of 0.3-1.2 chains/nm<sup>2</sup> can be routinely achieved by surface-initiated "living" polymerization.

**Scheme 2.** Synthesis of HNPs: (A) "Grafting To", (B) "Grafting From", (C) Polymer Micelle-Templated Synthesis, (D) Mixed Brush NPs,<sup>2</sup> and (E) Hairy Mesoporous NPs.<sup>47</sup>



Moreover, chain extension from the surface macroinitiator on NPs allows for the synthesis of grafted block copolymers, adding another dimension to HNPs and enriching their structures and properties.<sup>22,23</sup> By combining two different, compatible "living"/controlled polymerization techniques, it is possible to synthesize bicomponent polymer brush-grafted NPs, such as binary

mixed brushes and Janus HNPs (Scheme 1B). For example, we developed a robust method to synthesize well-defined mixed brushes on silica particles by sequential surface-initiated ATRP and NMRP, which are performed under different conditions.<sup>63</sup> To ensure that the grafting sites of two homopolymers are well mixed on the particle surface, we designed an asymmetric difunctional initiator that contains both initiating moieties for ATRP and NMRP (Scheme 2D).<sup>2</sup> The molecular characteristics (such as chain lengths, overall grafting densities, etc.) of the two grafted polymers in the brush layer can be tuned, allowing for study of their effects on microphase separation of mixed brushes.<sup>24,25,50,64-67</sup> However, a drawback of "grafting from" is that accurate determination of the molecular characteristics of the grafted polymers requires the cleavage of the grafted polymers from HNPs for conventional polymer characterizations such as SEC and <sup>1</sup>H NMR spectroscopy.<sup>34,58,63</sup>

(iii) Polymer Micelle-Templated Synthesis. Polymer micelle-templated synthesis of HNPs represents the third approach. In this method, a precursor, commonly a metal salt or an organometallic compound, is loaded into the core of polymer micelles, either multimolecular block copolymer or unimolecular star block micelles, followed by the reduction of (complex) metal ions in the micelle core to produce NPs or the reaction of (complex) metal ions with a later-added reactant (e.g., to form semiconductor quantum dots). Although the process is straightforward, one issue that has been observed is the formation of multiple NPs in the core of multimolecular micelles. In contrast, with the use of unimolecular star block copolymer micelles, this method has recently achieved a greater success in the synthesis of HNPs with uniform sizes, various shapes, and unusual morphologies (e.g., hollow hairy NPs). It is worth noting here that the number of grafted polymer chains is pre-determined by the number of the arms in the unimolecular micelles.

formation of multiple NPs in the core of multimolecular micelles and the rather low polymer grafting density in HNPs template-synthesized from unimolecular micelles, the following discussion on characterization of HNPs will be focused on those made from "grafting from" and "grafting to".

# **Characterization of HNPs – Determining Basic Characteristics**

The behaviors and properties of HNPs in liquid media and polymer matrices and as matrix-free nanocomposites are governed by the basic structural characteristics of both grafted polymers and core NPs. These include: molecular weight, molecular weight distribution, chemical composition and grafting density for grafted polymers; size, geometry and morphology for core NPs; and specific surface area if NPs are mesoporous or hollow. Determining these parameters is not only critical for the applications of HNPs but also important for optimizing the reaction conditions for the preparation of HNPs and developing new synthetic methods.

Molecular Weight, Molecular Weight Distribution (or Polydispersity Index (PDI) or Dispersity ( $\mathcal{D}$ )), and Degree of Polymerization (DP) of Grafted Polymer. Polymers are polydisperse, and as such, number average ( $M_n$ ) and weight average molecular weights ( $M_w$ ) are used to describe the average molar mass of a synthetic polymer, and the ratio of  $M_w/M_n$  represents the breadth of the molecular weight distribution, which is called polydispersity index (PDI) or dispersity ( $\mathcal{D}$ ). The values of  $M_n$ ,  $M_w$ , and  $\mathcal{D}$  are commonly determined by SEC (also called gel permeation chromatography), where polymer molecules are separated according to their hydrodynamic volume (size) in a series of columns packed with polymer beads containing pores of various sizes. <sup>69</sup> If the SEC is equipped with a triple detector system consisting of a multi-angle laser light scattering detector, a differential refractive index (RI) detector, and a viscometer,

absolute  $M_n$  and  $M_w$ , D, and other molecular characteristics such as intrinsic viscosity and radius of gyration ( $R_g$ ) can be obtained. For more common SEC systems with only a RI detector, the  $M_n$  and the D are usually reported relative to a set of narrow disperse polymer standards with known molecular weights (e.g., linear polystyrene (PS)); the reported  $M_n$  is basically the molecular weight of the polymer standard having the same hydrodynamic volume in the same solvent at the specified temperature.

For HNPs made by "grafting to", the molecular characteristics can be conveniently determined by SEC prior to the preparation of HNPs. For the brushes made by "grafting from", the grafted polymer has to be cleaved off from the core NPs for SEC analysis, which can be accomplished by using a chemical reagent to dissolve the core NPs or break a bond between the particle surface and the grafted chains (Figure 1A). 58,63 For example, HF is widely used to etch silica (nano)particles, 63 and iodine is used to cleave the gold-sulfur bond to degraft polymer chains.<sup>27</sup> More recently, ultrasonication was employed to mechanochemically activate the mechanophore at the core NPbrush interface to cleave the grafted polymer chains in mechanoresponsive HNPs. 71,72 It is important to note that the reaction used to cleave the grafted polymer should not affect the integrity of the polymer. A common practice in the synthesis of HNPs by surface-initiated "living" radical polymerization is to add a corresponding free initiator or CTA into the polymerization mixture, which produces a free analogous polymer in the solution. By cleaving polymer brushes off from the particles through, e.g., HF etching of silica NPs or cleavage of a bond in the surface-tethered initiator (e.g., benzyl ether linkage by (CH<sub>3</sub>)<sub>3</sub>SiI<sup>58</sup>), many researchers have observed that the molecular weights and dispersities of the grafted polymer in HNPs and the free polymer formed from the free initiator or CTA are very similar to each other (Figure 1B). <sup>23,34,58,63,71-73</sup> This allows for convenient characterization of molecular parameters of the grafted polymer without degrafting

as the separation of HNPs and the free polymer can be easily achieved by centrifuge. We note here that the situation for flat surfaces, however, may be different. Using computer simulations, 74,75 Genzer et al. observed a higher dispersity and a lower molecular weight for the grafted polymer compared to the free polymer, which was attributed to the surface confinement and crowding of grafted chains on the flat surface during the surface-initiated "living"/controlled radical polymerization.

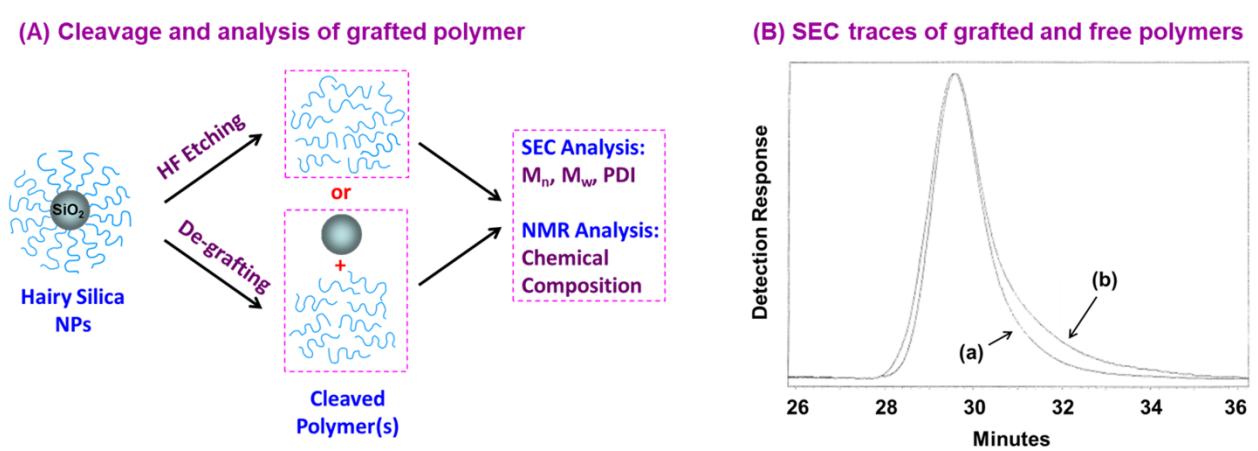


**Figure 1.** (A) Cleavage of grafted polymers from NPs for SEC analysis. (B) Comparison of SEC traces of (a) the grafted PS cleaved from silica gel (HNPs made by surface-initiated NMRP) and (b) the free PS from the free initiator. Adapted with permission from ref. 58. Copyright (1999) American Chemical Society.

Because the molecular weights of polymers are often reported as relative molecular weights with respect to polymer standards, it is necessary to determine the degree of polymerization (DP, the average number of monomer units per chain) of the grafted polymer for the calculation of grafting density. For polymers synthesized by "living" polymerizations such as ATRP, NMRP, RAFT,  $^{76-78}$  the DP can be calculated from the monomer conversion and the monomer-to-initiator or -CTA molar ratio, DP = conv.% × [M]<sub>0</sub>/[I]<sub>0</sub> or conv.% × [M]<sub>0</sub>/[CTA]<sub>0</sub> (for RAFT polymerization), where [M]<sub>0</sub>, [I]<sub>0</sub>, and [CTA]<sub>0</sub> are the initial concentrations of monomer, initiator, and CTA, respectively. The monomer conversions are usually measured by <sup>1</sup>H NMR spectroscopy using characteristic peaks of monomer and polymer (e.g., the peak position of -CH<sub>2</sub>- in the ester

group of a (meth)acrylate monomer shifts upfield after the polymerization 79,80) or a deliberately added reagent as internal reference. Theoretically, the surface-immobilized initiator/CTA moieties that successfully initiate polymerization (effective surface initiator/CTA) should be taken into calculation, particularly when the amount of surface initiator/CTA is not negligible compared with free initiator/CTA (e.g., in the case of NPs with a size of a few tens of nanometers). It is important to emphasize that one should not simply use the amount of surface-fixed initiator/CTA plus that of free initiator/CTA for the DP calculation, because not all surface initiator/CTA groups successfully start a polymer chain due to the steric hindrance and side reactions in the confined space. In our research, we determined the amount of effective surface initiator/CTA by comparing the amount of the grafted polymer to the total amount of the polymer formed.<sup>79</sup> The former is estimated from the amount of initiator/CTA-functionalized NPs added into the reaction mixture and the polymer content of HNPs from thermogravimetric analysis (TGA), and the latter is calculated from the initial quantity of monomer and the monomer conversion. Note that the underlying assumption for this method of calculating the DP is that the polymerization is "living". Certainly, the DP can be calculated directly from the absolute M<sub>n</sub> measured by SEC equipped with triple detectors. 81 For conventional SEC with a RI detector, if the polymer to be analyzed is the same type of calibration standards, the DP can also be directly calculated from the M<sub>n</sub>.<sup>63</sup>

Chemical Composition of Grafted Polymer. <sup>1</sup>H NMR spectroscopy is a key technique for analyzing the chemical composition of grafted polymer chains in HNPs. When the core NPs are small, with a diameter of < a few tens of nanometers, accurate quantitative analysis can be performed by <sup>1</sup>H NMR spectroscopy without cleavage of the grafted polymer from NPs. <sup>82,83</sup> For larger particles with a size of, e.g., 180 nm, <sup>63</sup> de-grafting of tethered chains is necessary because the broadening of the <sup>1</sup>H NMR peaks of grafted polymers impacts quantitative analysis. A

distinction should be drawn between homografted and heterografted HNPs; the former refers to the system in which there is only one type of grafted polymer chains, either homopolymer, random copolymers or block copolymers, while for heterografted NPs there are two or more types of chemically distinct grafted polymers. The molar ratio of different monomer units in random copolymers and the block length ratio of block copolymers in homografted systems can be calculated from the <sup>1</sup>H NMR spectra, as long as characteristic peaks for different monomer units can be identified.<sup>79</sup>

For heterografted HNPs such as binary mixed brush-grafted, bicomponent brush Janus and patchy NPs, <sup>63,81-83</sup> there is one additional variable: molar ratio of different types of polymer chains. Because <sup>1</sup>H NMR spectroscopy analysis only gives the molar ratio of different monomer units, other characterization methods have to be used to determine the DP of each polymer in order to calculate the molar ratio of different types of polymer chains. If one or more grafted polymers are made by surface-initiated "living" polymerization, the DP can be calculated from the monomer conversion and the monomer-to-sum of free initiator + effective surface initiator as discussed earlier. For example, we previously synthesized mixed poly(tert-butyl acrylate) (PtBA)/PS brushes on 180 nm silica particles by sequential surface-initiated ATRP and NMRP (Scheme 2D).<sup>63</sup> To determine the ratio of grafted PtBA to PS chains, HF was used to etch the silica core, and the degrafted polymers were analyzed by <sup>1</sup>H NMR spectroscopy. From the integrals of the peaks at 6.20 -7.20 ppm (5 aromatic hydrogen atoms of PS and the peak at 2.20 ppm (-CH- of PtBA), the molar ratio of PS to PtBA monomer units was 1.28: 1. Taking into consideration the DPs of two polymers, the ratio of grafted PS to PtBA chains was 1.06: 1, which is the ratio of their individual grafting density.<sup>63</sup> This method can be applied to determine the grafting density ratio of two grafted polymers in Janus bicomponent brush-grafted Au NPs, where <sup>1</sup>H NMR analysis can be performed

directly on HNPs in a good solvent.<sup>27,82,83</sup> As can be seen from above discussion, although <sup>1</sup>H NMR spectroscopy can reveal the chemical compositions of heterografted multicomponent HNPs, to determine the numbers and molar ratio of different types of polymer chains and other molecular characteristics, additional information, such as synthetic methods, DPs, etc., is needed.

Grafting Density of Polymer Chains in HNPs. The grafting density of polymer chains tethered on core NPs (σ, in units of chains/nm<sup>2</sup>) is a critical parameter for HNPs, which, along with molecular weight, determines whether the grafted chains are in the mushroom (noninteracting) or brush (stretched) regime and dictates the behavior of HNPs in solvents and in polymer matrices. For flat substrates, if tethered chains are in the mushroom regime, the thickness, L, is independent of  $\sigma$  ( $L \propto \sigma^0$ ). 84,85 With increasing  $\sigma$ , the grafted chains begin to interact with each other and enter the brush regime (more precisely, "semi-dilute" brush regime), where  $L \propto \mathrm{DP} \times \sigma^{1/3}$ . <sup>84,85</sup> At even higher grafting density ("concentrated" brush regime), theoretical analysis predicts a slightly different scaling relationship,  $L \propto \mathrm{DP} \times \sigma^{1/2.85}$  A salient characteristic of both "semi-dilute" and "concentrated" brushes is that L increases linearly with DP; the tethered chains are stretched compared with free polymer chains in good solvents (radius of gyration  $R_{\rm g} \propto {\rm DP}^{2/3}$ ). <sup>84,85</sup>  $R_{\rm g}$  is the root-mean-square, mass-weighted average distance of monomer units from the center of mass of a polymer chain<sup>69</sup> and is commonly used to describe the size of a polymer. To determine if grafted chains are in the mushroom or brush regime, reduced grafting density  $\tilde{\sigma}$ , defined as  $\sigma \pi R_{\rm g}^2$ , is often used.  $\tilde{\sigma}$  is the number of tethered chains in the area of  $\pi R_{\rm g}^2$ , an area covered by a free chain under the same conditions. Using crystal surface engineering of semicrystalline-amorphous diblock copolymers, Cheng et al. found that the tethered polymer begins to stretch at  $\tilde{\sigma} = 3.7-3.8$  and the highly stretched regime starts at  $\tilde{\sigma} = 14.3.^{86,87}$  Although these criteria are obtained from and used

for tethered chains on flat surfaces, they can be used as a guide for HNPs, especially those with relatively large core NPs.

Unlike tethered chains on a flat substrate, where  $\sigma$  does not vary with the distance from the substrate, the effective grafting density,  $\sigma^*$ , of grafted chains on NPs changes with increasing the distance from the NP surface. For spherical NPs,  $\sigma^*$  can be calculated according to  $\sigma^* = \sigma [r_0/r]^2$ , where  $r_0$  and r are the diameter of core NP and the distance from the NP center, respectively, and  $\sigma$  is the grafting density at the surface of core NPs. In the case of HNPs with a core NP size of < a few tens of nanometers and long grafted chains, the decrease in  $\sigma^*$  can be quite large and can trigger a transition of grafted chains from a "concentrated" brush regime to a "semi-dilute" brush regime. Using surface-initiated ATRP from 15.4 nm silica NPs, Choi et al. synthesized a series of HNPs with various molecular weights and observed by TEM of HNP monolayers that the dependence of NP surface-to-surface distance d on DP of grafted polymer ( $d \propto DP^x$ ) changed from x = 0.81 for relatively short chains to 0.52 for long chains (Figure 2).<sup>88</sup> The former corresponds to the "concentrated" brush regime, while the latter represents the characteristic of the semi-dilute brush regime; these observations are in good agreement with theoretical predictions from a modified Daoud and Cotton model. 89,90 Note that different brush regimes determine the mechanical properties of bulk HNPs, for example, brittle versus tough, as reported by Choi et al. 88,91

The  $\sigma$  of HNPs is commonly calculated by using the TGA data, the  $M_n$  of grafted polymer, and the surface area of core NP according to eq. (1):

$$\sigma = \frac{m_{Polymer}N_A}{M_n A} \tag{1}$$

where  $m_{\text{polymer}}$  is the mass of grafted polymer in one single HNP,  $N_A$  is the Avogadro number, and A is the surface area (nm<sup>2</sup>) of one core NP. TGA is a type of thermal analysis, in which the mass of a sample is measured as a function of increasing temperature usually at a constant heating rate

in a controlled atmosphere (air or  $N_2$ ). At sufficiently high temperatures, the grafted polymer decomposes into small molecules, leaving behind core NPs and thus providing the mass ratio of grafted polymer and core NPs after the correction for the organic component introduced in the initiator or CTA immobilization step. The mass of a single core NP can be readily calculated from its density and size, assuming a regular shape (spherical, rod-like, etc.), and thus we can determine the  $m_{polymer}$  in a single HNP.

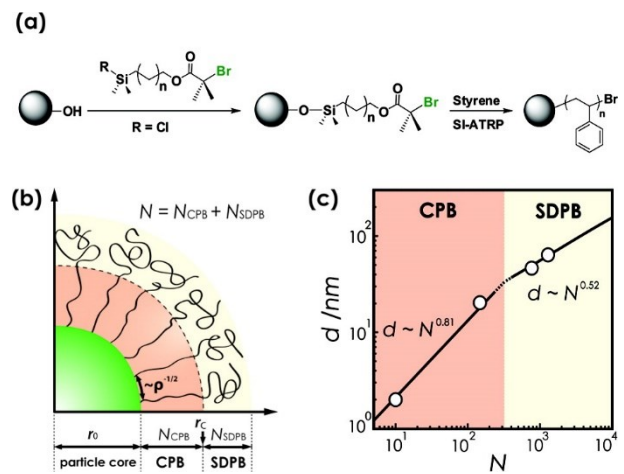


**Figure 2.** (a) Synthesis of HNPs by surface-initiated ATRP. (b) Schematic illustration of "concentrated particle brush" (CPB) and "semidilute particle brush" (SDPB) regimes. (c) Dependence of particle surface-to-surface distance d on DP (N) of grafted polymer chains determined by TEM analysis of HNP monolayers. Reproduced with permission from ref. 88. Copyright (2010) American Chemical Society.

For homografted HNPs, if the value of  $M_n$  is known, the  $\sigma$  can be calculated according to eq. (1). For heterografted HNPs such as binary mixed brush-grafted NPs and bicomponent brush-grafted Janus NPs, it is necessary to report the individual grafting density of each type of polymer chains. <sup>63-67</sup> If such HNPs are prepared in a step-wise fashion, then the  $\sigma$  of the first grafted polymer can be calculated first using eq. (1); the  $\sigma$  of the second polymer can be determined by the same method except the use of the increase in polymer content of HNPs. Alternatively, we can first determine the molar ratio of two types of monomer units by <sup>1</sup>H NMR analysis and then calculate

their mass ratio.  $^{81-84}$  By using this mass ratio and the polymer content from TGA, we can determine  $m_{\text{polymer}}$  for each polymer and thus their individual grafting densities.

Characteristics of Core NPs. The characteristics of core NPs that are important to the behavior, properties, and applications of HNPs include size, shape (spherical, cubic, etc.), morphology (solid, mesoporous, or hollow), and specific surface area (for porous and hollow particles). TEM is an indispensable tool for determining the characteristics of solid and porous NPs, and ImageJ software is widely used to obtain the average size and standard deviation of NPs from TEM images. In TEM, an electron beam is transmitted through a sample with a thickness of  $\sim 100$  nm or less, and the electrons that pass through the sample form an image. The contrast observed in TEM micrographs often comes from different abilities to absorb or scatter incident electrons caused by the composition (density) or thickness variations in the sample, with darker areas corresponding to more electron losses. 92 TEM has the capability to image at atomic and subatomic levels, and the resolution is thousands of times higher than that of optical microscopes because the wavelength of electrons is much shorter than visible light. As-synthesized core NPs have a high tendency to aggregate, which could occur during the TEM sample preparation, making it difficult to image individual NPs. In contrast, HNPs can readily form a monolayer on carboncoated TEM grids mediated by the grafted polymer, and it is easier to measure the sizes of core NPs because grafted chains are "invisible" due to their much lower ability to absorb/scatter electrons. 11,34 While TEM is a powerful imaging technique, the specimen must be very thin (~ 100 nm or less) and ultramicrotomy is often used to cut samples to an appropriate thickness.<sup>64</sup> For small HNPs, there is no need to use ultramicrotomy as drop casting of a dilute dispersion of HNPs in a good solvent affords a monolayer readily, which is suitable for TEM visualization. 11,34 Another drawback of TEM is that only a very limited number of NPs can be visualized at one time. Thus,

it is necessary to acquire images of a sufficiently large number of NPs to generate statistically meaningful results.

Porous NPs hold great potential in a variety of applications, including drug delivery and gas separation. Separation. Porous materials can be classified into mesoporous (pore diameters: 2-50 nm), microporous (pore sizes: <2 nm), and macroporous (with pores >50 nm), for which specific surface area ( $m^2/g$ ) is a critical parameter and is usually measured by the gas adsorption-desorption method based on the Brunauer–Emmett–Teller (BET) theory. The BET theory extended the Langmuir theory for the monolayer adsorption of gas molecules to multilayer adsorption, allowing for the determination of the quantity of adsorbed monolayer gas molecules ( $\nu_m$ ) and thus the specific surface area ( $S_{BET}$ ). Nitrogen is the most commonly used gas adsorbate, and the quantity (volume) of  $N_2$  gas ( $\nu$ ) adsorbed to the surface of fully dried porous NPs is measured at the boiling point of liquid nitrogen (77 K) at a series of equilibrium pressures (p). The  $\nu_m$  can be calculated from eq. (2): $^{97}$ 

$$\frac{1}{v\left[\left(\frac{p_0}{p}\right)-1\right]} = \frac{c-1}{v_m c} \left(\frac{p}{p_0}\right) + \frac{1}{v_m c} \tag{2}$$

where  $p_0$  is the saturation pressure of adsorbate at the temperature of adsorption, and c is the BET constant, which is related to the heat of adsorption. To determine  $v_m$ , one can make a plot of  $1/\{v[(p_0/p)-1]\}$  against  $(p/p_0)$  (BET plot). The value of  $v_m$  can be calculated from the slope and the y-intercept ( $v_m = 1/(\text{slope} + \text{intercept})$ ). The total surface area ( $S_{\text{total}}$ ) and  $S_{\text{BET}}$  can be calculated by using eq. 3 and 4:

$$S_{total} = \frac{v_m N_A s}{V} \tag{3}$$

$$S_{BET} = \frac{S_{total}}{a} \tag{4}$$

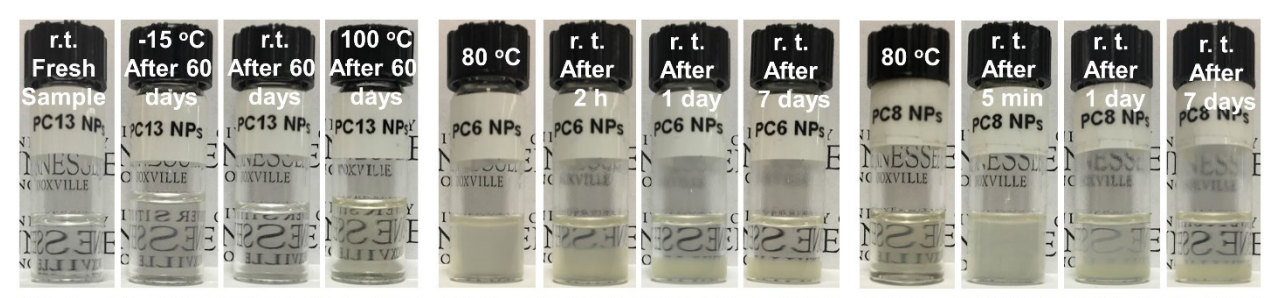
where s is the adsorption cross section of the gas molecule, V is the molar volume of gaseous adsorbate, and a is the mass of the porous materials.

While hairy porous NPs are envisioned to have potential in a variety of applications, particularly delivery of substances, grafting polymer chains only at the exterior surface of NPs (i.e., preserving internal pores) has been challenging. If an initiator is immobilized on the surface of porous NPs, both exterior and interior surfaces would be modified, and thus surface-initiated polymerization would also occur inside the pores, which would greatly decrease the specific surface area. Since porous NPs are commonly synthesized by using micelles as template, this problem can be mitigated by modifying the exterior surface of NPs prior to the removal of micelles,<sup>47</sup> as reported by Hong et al. (Scheme 2E). However, their results showed that after the growth of polymer chains the  $S_{\text{BET}}$  decreased significantly (from 1130 to 350 m<sup>2</sup>/g) and the amount of the grafted polymer was small. If a facile method is discovered, the potential of porous HNPs can be better explored.

## **Characterization of HNPs – Probing Their Behavior in Solvents**

The dispersibility of HNPs in solvents and their behavior in solution in response to environmental changes are vital to their functions, properties, and formation of self-assembled hierarchical structures. With the aid of gentle shaking, stirring, or ultrasonication, HNPs can be readily dispersed in good solvents for the grafted polymers if the polymer chains are sufficiently long and/or the grafting density is high enough. The stability of HNPs in good solvents stems from the favorable enthalpic interactions between grafted chains and solvent and the steric (entropic) interactions between HNPs, which counteract and screen the van der Waals attractive forces between NPs, leading to an overall repulsive effect among HNPs. 98

The dispersibility and stability of HNPs in solvents can be characterized by various techniques. The simplest one is visual inspection (Figure 3). <sup>99</sup> If HNPs cannot be dispersed in a solvent over an extended period of time by stirring or ultrasonication, it can be easily seen with the naked eye (Figure 3B). The homogeneous dispersions of HNPs in good solvents resemble molecular solutions (Figure 3A) and can be clear or slightly opaque depending on the concentration and core NP size as well as the RIs of core NPs and the solvent. If HNPs gradually aggregate, the dispersions may become cloudier and a precipitate may eventually appear (Figure 3C). Gold NPs often exhibit different colors in the dispersed and aggregated states, <sup>82</sup> which result from the changes in surface plasmon resonance of Au NPs in different states and can be measured with UV-vis spectrometry.



(A) 1 wt% PC13-NP1-9.7k in PAO (B) 1 wt% PC6-NP1-7.0k in PAO (C) 1 wt% PC8-NP1-7.8k in PAO

**Figure 3.** Optical photos of (A) a 1 wt% fresh dispersion and three 1% dispersions of poly(tridecyl methacrylate)-grafted, 23 nm silica NPs with  $M_{n,SEC}$  of 9.7 kDa (PC13-NP1-9.7k) in PAO after 60 days at -15 °C, r.t., and 100 °C; (B) a 1% dispersion of poly(n-hexyl methacrylate)-grafted silica NPs with  $M_{n,SEC}$  of 7.0 kDa (PC6-NP1-7.0k) in PAO at 80 °C and at r.t. for 2 h, 24 h, and 7 days after removal from an 80 °C oil bath; (C) a 1% dispersion of poly(2-ethylhexyl methacrylate)-grafted silica NPs with  $M_{n,SEC}$  of 7.8 kDa (PC8-NP1-7.8k) in PAO at 80 °C and at r.t. for 5 min, 1 day, and 7 days after removal from an 80 °C oil bath. Reproduced with permission from ref. 99. Copyright (2017) American Chemical Society.

The hydrodynamic size ( $D_{\rm H}$ ) of HNPs in a good solvent, which can be measured by dynamic light scattering (DLS),<sup>69</sup> is usually much larger than that of core NPs because of the swelling of polymer brushes and the polydispersity of grafted chains.<sup>99,100</sup> Note that even if a dispersion of HNPs in a solvent is totally transparent, it may not mean that the HNPs are individually dispersed. DLS and TEM are commonly used together to determine if the particles are fully dispersed in a

solvent. DLS measures the time dependence of the fluctuation in scattering intensity of particles in a solution, which originates from their Brownian motion – the random movement of NPs in a liquid caused by the continuous bombardment of surrounding solvent molecules. Smaller NPs move faster in a solvent, and the correlation function of scattered light intensity decays more rapidly. Conversely, larger particles diffuse slowly, and the correlation of the signal takes a longer time to decay. The light scattering intensity data can be analyzed to give the translational diffusion coefficient ( $D_t$ ) of particles, which can then be converted to the  $D_h$  of particles through the Stokes-Einstein equation:  $D_h = kT/(3\pi\eta D_t)$ , where k is the Boltzmann constant, T is absolute temperature,  $\eta$  is the viscosity of the medium.<sup>69</sup> For NPs with a shape other than spherical, the  $D_h$  obtained by DLS is basically the diameter of an equivalent sphere that has the same  $D_t$  as the particles in question.<sup>69</sup> Note that the shape information can be obtained from angle dependence of scattering intensity.

DLS can routinely measure the  $D_h$  of particles in the range from  $\sim 1$  nm to a few  $\mu m$  and is very powerful for studying the stability of particles in solution. Figure 4A and B shows a TEM image of PtBA-b-poly(n-butyl acrylate) brush-grafted, 15.8 nm silica NPs cast from a dispersion in tetrahydrofuran (THF) and their  $D_h$  distribution in THF from DLS, respectively;<sup>22</sup> clearly, the HNPs were fully dispersed in THF. Inorganic and metallic NPs are known to be an effective additive for lubricating oils for friction and wear reduction.<sup>33</sup> However, these NPs tend to aggregate and precipitate out from hydrophobic oils.<sup>33</sup> We recently developed oil-soluble polymergrafted silica and titania NPs, which exhibited excellent dispersibility in polyalphaolefin (PAO),<sup>11</sup> a widely used synthetic oil for engine lubrication. The HNPs were highly stable in PAO in the temperature range from – 15 to 100 °C, as shown from DLS measurements of HNP size after the dispersions were stored at -15, 18, and 100 °C for 60 days (Figure 4C). A single size distribution

was observed for each sample, and the average  $D_h$  values were 54.4 nm (-15 °C), 57.5 nm (18 °C), and 58.9 nm (100 °C), which were essentially the same as that (56.2 nm) for the freshly prepared sample.<sup>99</sup>

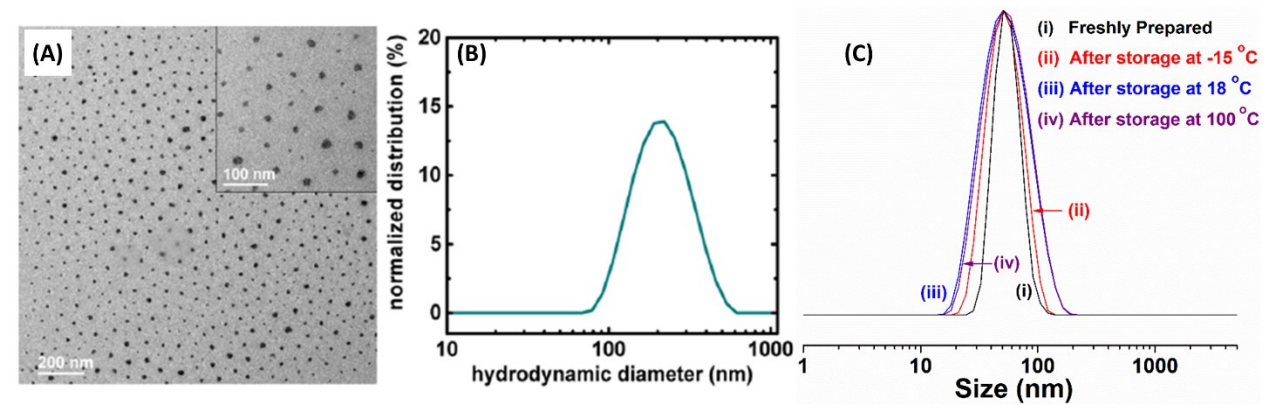


**Figure 4.** (A) TEM image and (B) DLS  $D_h$  distribution of 15.8 nm silica NPs grafted with poly(t-butyl acrylate)-b-poly(n-butyl acrylate) brushes. The TEM sample was prepared by solution casting of a 1 mg/mL dispersion of HNPs in THF. Adapted with permission from ref. 22. Copyright (2017) American Chemical Society. (C) DLS  $D_h$  distributions of PC13-NP1-9.7k, measured at 23 °C, in a fresh dispersion in PAO (i) and in PAO after 60 days at -15 °C (ii), room temperature (18 °C) (iii), and 100 °C (iv). Reproduced with permission from ref. 99. Copyright (2017) American Chemical Society.

DLS is widely used to study the behavior of stimuli-responsive HNPs in water upon application of an external stimulus (e.g., temperature or pH changes, etc.).  $^{43,79,80}$  Among various such materials, thermoresponsive HNPs are the most studied. Given that the effective grafting density decreases when moving away from the surface of core NPs, it would be interesting to probe how thermoresponsive brushes on NPs collapse upon heating. Using surface-initiated ATRP, Wu et al. synthesized thermosensitive poly(*N*-isopropylacrylamide) (PNIPAM)-grafted, 70 nm silica NPs and studied the thermally-induced lower critical solution temperature (LCST) transition in water. DLS showed that the PNIPAM HNPs exhibited two-stage shrinking upon heating, in contrast to the sharp LCST transition of free PNIPAM. The hydrodynamic radius  $\langle R_h \rangle$  first decreased monotonically in the temperature range of 20–29 °C, followed by a sharp decrease from 31 to

37 °C (Figure 5a). The two-stage transition can also be seen from the plot of  $R_g$ , measured by static light scattering, versus temperature (Figure 5b). The first transition was attributed to the n-cluster-induced collapse of the inner zone of PNIPAM brushes, and the  $2^{nd}$  transition was ascribed to the collapse of the brushes' outer region, which had a lower segment density compared with the inner zone. Tenhu et al. used micro-differential scanning calorimetry to study the grafted PNIPAM chains on small gold NPs and also observed double transitions.  $^{101}$ 

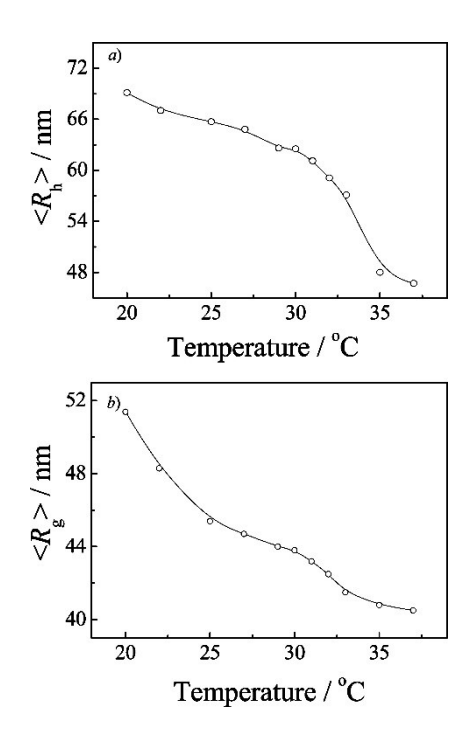


**Figure 5.** Temperature dependence of (a) hydrodynamic radius  $\langle R_h \rangle$  and (b)  $\langle R_g \rangle$  obtained for 5 × 10<sup>-6</sup> g/mL aqueous solution of PNIPAM brush-grafted, 70 nm silica NPs. Reproduced with permission from ref. 43. Copyright (2008) American Chemical Society.

# Characterization of HNPs – Elucidating the Self-Assembled Structures of Multicomponent Brush HNPs

Multicomponent polymer brush-grafted NPs have received considerable interest in recent years, owing to their abilities to undergo chain reorganization within the brush layer in response to environmental changes, exhibiting distinct nanostructures under different conditions, and to self-assemble into hierarchical structures such as vesicles and tubules. <sup>27,63-67,81-83,102-104</sup> Examples of such HNPs include binary mixed polymer- and diblock copolymer-grafted NPs as well as bicomponent brush Janus NPs. The most important analytical tool for characterizing the self-assembled structures of multicomponent brush NPs is electron microscopy, including scanning electron microscopy (SEM), TEM, and TEM electron tomography (ET). <sup>105</sup> A SEM image is acquired by using a focused beam of electrons to raster-scan the sample surface, allowing for characterization on a length scale from nanometers to micrometers. SEM images are formed either by secondary electrons, which are mainly generated by interactions of incident electrons with the sample, or backscattered electrons, which are elastically scattered out of the sample with a significant percentage traveling back along the incident beam. While higher resolutions are usually achieved by using secondary electrons due to their confinement to the volume near the beam-impacted area, backscattered electrons give a better compositional contrast, with heavier elements appearing brighter in the image. <sup>105</sup>

TEM is routinely used to study the morphologies of multicomponent block copolymers along with small angle X-ray scattering and other characterization techniques. The contrast between different polymer domains under TEM is usually low, and selective staining of one block that contains carbon-carbon double bonds or aromatic rings with a heavy metal oxide, such as RuO<sub>4</sub> or OsO<sub>4</sub>, is commonly used to enhance the contrast. For example, in the study of mixed PtBA/PS brush-grafted silica particles synthesized by surface-initiated ATRP and NMRP (Scheme 2D), no microphase separation was observed without staining.<sup>64</sup> After staining of microtomed thin sections or a solution-cast monolayer of HNPs with RuO<sub>4</sub> vapor, lateral microphase separation of the brushes became visible, where the PtBA microdomains appeared bright and the PS domains appeared dark (Figure 6).<sup>64-67</sup> This allowed us to study the effects of selective solvent, molecular

weight, grafting density, and substrate curvature on periodicity (or feature size) of micropatterns, revealing the intriguing behavior of mixed brushes; one example is shown in Figure 6A and B, where the feature size became significantly smaller with increasing the overall grafting density of mixed brushes.<sup>67</sup>

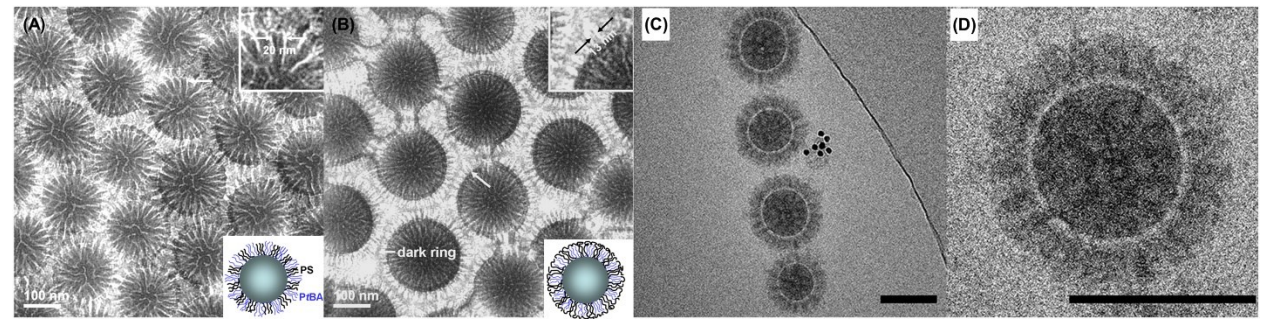


**Figure 6.** TEM micrographs of (A) mixed PtBA/PS brush-grafted silica particles (PtBA  $M_n$  = 24.5 kDa,  $\sigma_{PtBA}$  = 0.36 chains/nm²; PS  $M_n$  = 24.9 kDa,  $\sigma_{PS}$  = 0.27 chains/nm²;  $\sigma_{total}$  = 0.63 chains/nm²; DP<sub>PS</sub>/DP<sub>PtBA</sub> = 1.25) and (B) mixed PtBA/PS brush-grafted particles (PtBA  $M_n$  = 23.7 kDa,  $\sigma_{PtBA}$  = 0.48 chains/nm²; PS  $M_n$  = 25.7 kDa,  $\sigma_{PS}$  = 0.51 chains/nm²;  $\sigma_{total}$  = 0.99 chains/nm²; DP<sub>PS</sub>/DP<sub>PtBA</sub> = 1.31) after casting from a CHCl<sub>3</sub> dispersion and staining with RuO<sub>4</sub> vapor at r.t. for 20 min. Adapted with permission from ref. 67. Copyright (2010) American Chemical Society. (C) Cryoelectron micrograph of mixed PAA/PS brush-grafted silica NPs in DMF and (D) one enlarged NP in (C). The PAA chains were stained by uranyl acetate to bear a darker contrast. The scale bars represent 100 nm. Adapted with permission from ref. 109. Copyright (2015) American Chemical Society.

While powerful, conventional TEM (2-D TEM) actually projects 3-dimensional (3-D) nanostructures onto a 2-D plane, which does not allow for discerning the spatial arrangements of different components in the 3-D space. The continuous development of electron microscopy has made it possible to visualize detailed 3-D structures, and this is achieved through ET. 106-109 Tomography is a term used to describe a process of "images by sections". 106 A series of TEM images are acquired at different tilting/viewing angles, most commonly by using the single-axis scheme, where the sample rotates around a fixed axis from one extreme to another extreme angle at constant tilt increments. The maximum tilt angle is usually restricted to +/- 70° due to the

shadowing of the specimen holder and the limited space in the chamber. The 2-D projected images acquired from different tilting angles are then aligned and reconstructed to produce a 3-D structure.

Dispersing inorganic NPs into polymer matrices is critical for making advanced polymer nanocomposites with improved properties,<sup>5-7</sup> and grafting polymers onto the NPs has been shown to be an effective method to achieve uniform dispersion of NPs in polymers. Using TEM-ET, Tang et al. studied the behavior of mixed PtBA/PS brush-grafted, 67 nm silica NPs with PtBA M<sub>n</sub> of  $22.2\ kDa$  and PS  $M_n$  of  $23.4\ kDa$  in selective homopolymer matrices with different molecular weights.<sup>35</sup> In the 5 kDa PtBA matrix, the HNPs are well dispersed (Figure 7A), and the PS microdomains are isolated, protruding out from the surface of the silica NP (Figure 7B and C). In contrast, in the 65 kDa PtBA matrix, the NPs aggregate into either strings or small flocculates, and the PS domains are more connected to form short worm-like structures in the average and above average sized NPs. These observations can be explained by the wet- and dry-brush theory. 110,111 When the  $M_n$  of PtBA matrix is much smaller than that of grafted PtBA, the PtBA matrix molecules penetrate into the brush layer and swell the PtBA domains. The swollen PtBA chains stretch out into the matrix, and the grafted PS collapse into isolated domains. When the matrix  $M_n$  is higher, the longer matrix PtBA chains cannot diffuse into the mixed brush layer, resulting in a morphology similar to the unperturbed morphology for the uniformly collapsed mixed brush-grafted NPs. These results demonstrated the responsive behavior of mixed brush particles in polymer matrices, providing a guide on the possible use of such multicomponent HNPs in the fabrication of polymer nanocomposites. It should be noted here that TEM only examines a very small fraction of a sample. To determine if HNPs are uniformly dispersed in a polymer matrix in the study of polymer nanocomposites, ultra-small-angle X-ray or neutron scattering is commonly used. 111,112

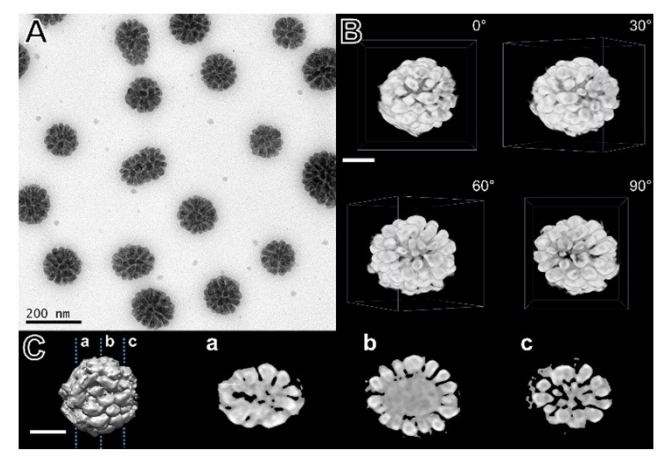


**Figure 7.** (A) TEM image of mixed PtBA/PS brush-grafted silica particles in 5 kDa PtBA matrix stained by RuO<sub>4</sub> for 20 min. (B) 3D TEM images (solid mode) of a reconstructed HNP in 5 kDa PtBA matrix at different rotation angles. (C) Cross-sectional scan images (surface mode) at positions a-c. PS is the visible phase. The scale bars in (B) and (C) are 50 nm. Reproduced with permission from ref. 35. Copyright (2015) Royal Society of Chemistry.

Electron microscopy is also critical for studying the hierarchical structures formed by self-assembly of multicomponent HNPs. Nie et al. synthesized amphiphilic diblock copolymer-grafted gold NPs and investigated their self-assembly behavior by using SEM, 2-D and 3-D TEM (Figure 8). Through the thin film hydration method, these HNPs self-assembled into vesicles and tubules mediated by the grafted diblock copolymer as revealed by SEM and TEM. The TEM images at multiple tilt angles (-60° to 60°) were recorded and are shown in Figure 8g. The 3-D images unequivocally showed vesicles with a hollow cavity created by a single layer of HNPs in the membrane. These hierarchical self-assemblies have potential applications in bioimaging and photothermal therapy due to the plasmon coupling in the assemblies.

Traditionally, TEM is performed on dried thin samples, whose structures may be different from the solvated/hydrated states as the nanostructures may undergo changes during the solvent evaporation. This problem can be circumvented by using cryogenic TEM,<sup>114</sup> where a solvated/hydrated sample is imaged in the frozen state. For example, the lateral microphase separation of mixed PS/poly(acrylic acid) (PAA) brush-grafted silica NPs in *N*,*N*-

dimethylformamide (DMF) is clearly observed by cryo-TEM (Figure 6C and D). <sup>109</sup> The cryo-TEM specimen is prepared by plunging a solvated sample-loaded TEM grid into a cryogen (e.g., liquid ethane) to vitrify the solvent and then quickly transferred to a liquid nitrogen-cooled high vacuum chamber of a transmission electron microscope for imaging. The selective staining should be performed before the plunge-freezing of the sample as one cannot stain the specimen in the vitrified solvent. ET can also be performed to generate the 3D structure in the frozen state (cryo-ET). <sup>114</sup> Cryo-TEM is very useful for obtaining information on the native state of a sample in a solvent; however, it is not easy to acquire high quality 2-D and 3-D cryo-TEM images as performing cryo-TEM requires extensive training and practice.

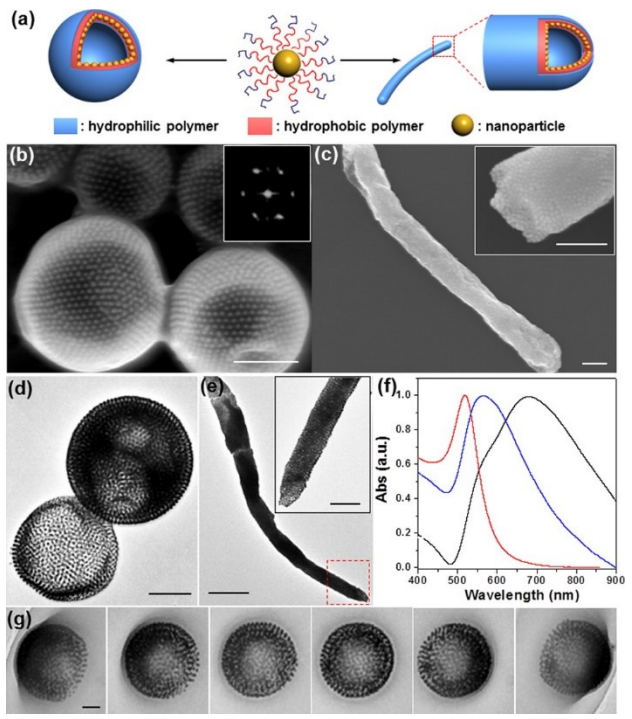


**Figure 8.** (a) Amphiphilic diblock copolymer-assisted self-assembly of Au NPs into vesicles or tubules. (b – e) SEM (b,c) and TEM (d,e) images of vesicles (b,d) and tubules (c,e) from self-assembly of gold NPs grafted with PS-*b*-poly(methoxydi(ethylene glycol) methacrylate) and PS-*b*-poly(ethylene oxide) chains, respectively. Inset in (b) is the FFT pattern of SEM image. (f) UV-vis spectra of individual Au NPs, vesicles, and tubules (from left to right). (g) TEM images of vesicles at different tilting angles (left to right:  $-60^{\circ}$ ,  $-40^{\circ}$ ,  $-20^{\circ}$ ,  $0^{\circ}$ ,  $30^{\circ}$ , and  $60^{\circ}$ ). Scale bars: 200 nm in (b-d) and insets of (c,e), 500 nm in (e), and 100 nm in (g). Reproduced with permission from ref. 113. Copyright (2012) American Chemical Society.

#### **Summary and Outlook**

HNPs are an important class of hybrid nanostructured materials, which hold promise in a variety of applications. To achieve full potential of HNPs in technologies and to understand the behavior of HNPs under various conditions, characterization is critical. This Feature Article aims to provide readers with an introduction on the determination of basic defining parameters, the behavior of HNPs in solvents, and self-assembled structures of multicomponent polymer-grafted NPs. The principles of characterization techniques are briefly introduced, and the limitations are pointed out when appropriate. Despite enormous progress being made, challenges remain, particularly for characterization of multicomponent HNPs. For heterografted HNPs with nonuniform distributions of distinct grafted polymers (e.g., Janus brush NPs and patchy HNPs), significant challenges in characterization exist, even for basic parameters. It is difficult to precisely determine the surface areas covered by different domains and the grafting densities of different polymers, although decoration with smaller metal NPs has been attempted to estimate the surface area of each domain in Janus HNPs.<sup>27</sup> The issue is further compounded by the responsive nature of grafted polymer chains on small HNPs, which can easily undergo conformational changes due to environmental variations. We believe that a concerted effort in the synthesis and characterization of these HNPs holds the key. For self-assembled nanostructures, even for one of the simplest multicomponent HNPs – binary mixed brushes on small NPs, the bulk morphologies have not been reported, although interesting nanostructures have been predicted by computer simulations. 102 It is our belief that ET will play a key role in elucidating the complex morphologies exhibited by multicomponent HNPs.

**Acknowledgments:** B.Z. thanks NSF for supporting his research work (DMR-1607076 and CHE-1709663).

#### **ORCID**

Bin Zhao: 0000-0001-5505-9390

### **Biographies of Authors**

Andrew J. Chancellor is a second-year graduate student working on well-defined multicomponent and also functional polymer brushes. Bryan T. Seymour finished his Ph.D. dissertation defense in the spring semester of 2019. His dissertation research focused on developing hairy nanoparticles as oil lubricant additive for friction and wear reduction. Bin Zhao is Paul and Wilma Ziegler Professor of Chemistry at the University of Tennessee Knoxville. His research interests include macromolecular brush materials, stimuli-responsive polymers, and liquid crystalline polymers.

#### **References:**

- 1. Pyun, J.; Matyjsazewski, K. Synthesis of Nanocomposite Organic/Inorganic Hybrid Materials Using Controlled/"Living" Radical Polymerization. *Chem Mater.* **2001**, *13*, 3436-3448.
- 2. Zhao, B.; Zhu, L. Mixed Polymer Brush-Grafted Particles: A New Class of Environmentally Responsive Nanostructured Materials. *Macromolecules* **2009**, *42*, 9369-9383.
- 3. Wu, L.; Glebe, U.; Böker, A. Surface-Initiated Controlled Radical Polymerizations from Silica Nanoparticles, Gold Nanocrystals, and Bionanoparticles. *Polym. Chem.* **2015**, *6*, 5143-5184.
- 4. Hui, C. M.; Pietrasik, J.; Schmitt, M.; Mahnoey, C.; Choi, J.; Bockstaller, M. R.; Matyjsazewski, K. Surface-Initiated Polymerization as an Enabling Tool for Multifunctional (Nano-)Engineered Hybrid Materials. *Chem. Mater.* **2014**, *26*, 745-762.
- 5. Kumar, S. K.; Jouault, N.; Benicewicz, B.; Neely, T. Nanocomposites with Polymer Grafted Nanoparticles. *Macromolecules* **2013**, *46*, 3199-3214.
- 6. Kumar, S. K.; Benicewicz, B. C.; Vaia, R. A.; Winey, K. I. 50<sup>th</sup> Anniversary Perspective: Are Polymer Nanocomposites Practical for Applications? *Macromolecules* **2017**, *50*, 714–731.
- 7. Fernandes, N. J.; Koerner, H.; Giannelis, E. P.; Vaia, R. A. Hairy Nanoparticle Assemblies as One-Component Functional Polymer Nanocomposites: Opportunities and Challenges. *MRS Commun.* **2013**, *3*, 13–29.
- 8. Zhang, L.; Bei, H. P.; Piao, Y.; Wang, Y.; Yang, M.; Zhao, X. Polymer-Brush-Grafted Mesoporous Silica Nanoparticles for Triggered Drug Delivery. *ChemPhysChem* **2018**, *19*, 1956-1964.
- 9. He, J.; Huang, X.; Li, Y.-C.; Liu, Y.; Babu, T.; Aronova, M. A.; Wang, S.; Lu, Z.; Chen, X.; Nie, Z. Self-Assembly of Amphiphilic Plasmonic Micelle-Like Nanoparticles in Selective Solvents. *J. Am. Chem. Soc.* **2013**, *135*, 7974–7984.
- 10. Liu, G.; Liu, Z.; Li, N.; Wang, X.; Zhou, F.; Liu, W. Hairy Polyelectrolyte Brushes-Grafted Thermosensitive Microgels as Artificial Synovial Fluid for Simultaneous Biomimetic Lubrication and Arthritis Treatment. *ACS Appl. Mater. Interfaces* **2014**, *6*, 20452–20463.
- 11. Wright, R.A.E.; Wang, K. W.; Qu, J.; Zhao, B. Oil-Soluble Polymer Brush-Grafted Nanoparticles as Effective Lubricant Additives for Friction and Wear Reduction. *Angew. Chem. Int. Ed.* **2016**, *55*, 8656-8660.

- 12. Tian, C. C.; Bao, C. H.; Binder, A.; Zhu, Z. Q.; Hu, B.; Guo, Y. L.; Zhao, B.; Dai, S. An Efficient and Reusable "Hairy" Particle Acid Catalyst for the Synthesis of 5-Hydroxymethylfurfural from Dehydration of Fructose in Water. *Chem. Commun.* **2013**, *49*, 8668-8670.
- 13. Ohno, K.; Morinaga, T.; Koh, K.; Tsujii, Y.; Fukuda, T. Synthesis of Monodisperse Silica Particles Coated with Well-Defined, High-Density Polymer Brushes by Surface-Initiated Atom Transfer Radical Polymerization. *Macromolecules* **2005**, *38*, 2137-2142.
- 14. Li, C.; Han, J.; Ryu, C. Y.; Benicewicz, B. C. A Versatile Method to Prepare RAFT Agent Anchored Substrates and the Preparation of PMMA Grafted Nanoparticles. *Macromolecules* **2006**, *39*, 3175–3183.
- 15. You, Y.-Z.; Kalebaila, K. K.; Brock, S. L.; Oupický, D. Temperature-Controlled Uptake and Release in PNIPAM-Modified Porous Silica Nanoparticles. *Chem. Mater.* **2008**, *20*, 3354-3359.
- Yavuz, M. S.; Cheng, Y.; Chen, J.; Colbey, C. M.; Zhang, Q.; Rycenga, M.; Xie, J.; Kim, C.; Schwartz, A. G.; Wang, L. V.; Xia, Y. Gold Nanocages Covered by Smart Polymers for Controlled Release with Near-Infrared Light. *Nat. Mater.* 2009, 8, 935-939.
- 17. Frischknecht, A. L.; Hore, M. J. A.; Ford, J.; Composto, R. J. Dispersion of Polymer-Grafted Nanorods in Homopolymer Films: Theory and Experiment. *Macromolecules* **2013**, *46*, 2856-2869.
- 18. Hotchkiss, J. W.; Lowe, A. B.; Boyes, S. G. Surface Modification of Gold Nanorods with Polymers Synthesized by Reversible Addition-Fragmentation Chain Transfer Polymerization. *Chem. Mater.* **2007**, *19*, 6–13.
- 19. Zhu, M.-Q.; Wang, L.-Q.; Exarhos, G. J.; Li, A. D. Q. Thermosensitive Gold Nanoparticles. *J. Am. Chem. Soc.* **2004**, *126*, 2656–2657.
- 20. Kizhakkedathu, J. N.; Norris-Jones, R.; Brooks, D. E. Synthesis of Well-Defined Environmentally Responsive Polymer Brushes by Aqueous ATRP. *Macromolecules* **2004**, *37*, 734–743.
- 21. Zhao, B.; Jiang, X. M.; Li, D. J.; Jiang, X. G.; O'Lenick, T. G.; Li, B.; Li, C. Y. Hairy Particle-Supported 4-*N*,*N*-Dialkylaminopyridine: An Efficient and Recyclable Nucleophilic Organocatalyst. *J. Polym. Sci. Part A: Polym. Chem.* **2008**, *46*, 3438-3446.
- 22. Chmielarz, P.; Yan, J.; Krys, P.; Wang, Y.; Wang, Z.; Bockstaller, M. R.; Matyjaszewski, K. Synthesis of Nanoparticle Copolymer Brushes via Surface-Initiated seATRP. *Macromolecules* **2017**, *50*, 4151–4159.
- 23. Wright, R. A. E.; Henn, D. M.; Zhao, B. Thermally Reversible Physically Crosslinked Hybrid Network Hydrogels Formed by Thermosensitive Hairy NPs. *J. Phys. Chem. B* **2016**, *120*, 8036-8045.
- 24. Bao, C. H; Tang, S. D.; Horton, J. M.; Jiang, X. M.; Tang, P.; Qiu, F.; Zhu, L.; Zhao, B. Effect of Overall Grafting Density on Microphase Separation of Mixed Homopolymer Brushes Synthesized from Y-Initiator-Functionalized Silica Particles. *Macromolecules* **2012**, *45*, 8027-8036.
- 25. Bao, C. H.; Tang, S. D.; Wright, R. A. E.; Tang, P.; Qiu, F.; Zhu, L.; Zhao, B. Effect of Molecular Weight on Lateral Microphase Separation of Mixed Homopolymer Brushes Grafted on Silica Particles. *Macromolecules* **2014**, *47*, 6824–6835.
- Wu, L.; Glebe, U.; Böker, A. Synthesis of Polystyrene and Poly(4-vinylpyridine) Mixed Grafted Silica Nanoparticles via a Combination of ATRP and Cu<sup>I</sup>-Catalyzed Azide-Alkyne Click Chemistry. *Macromol. Rapid Commun.* 2017, 38, 1600475.

- 27. Wang, B. B.; Li, B.; Zhao, B.; Li, C. Y. Amphiphilic Janus Gold Nanoparticles via Combining "Solid State Grafting to" and "Grafting-from" Methods. *J. Am. Chem. Soc.* **2008**, *130*, 11594-11595.
- 28. Berger, S.; Synytska, A.; Ionov, L.; Eichhorn, K.-J.; Stamm, M. Stimuli-Responsive Bicomponent Polymer Janus Particles by "Grafting from"/"Grafting to" Approaches. *Macromolecules*, **2008**, *41*, 9669–9676.
- 29. Khabibullin, A.; Kopec, M.; Matyjaszewski, K. Modification of Silica Nanoparticles with Miktoarm Polymer Brushes via ATRP. *J. Inorg. Organomet. Polym.* **2016**, *26*, 1292-1300.
- 30. Daniel, M.-C.; Astuc, D. Gold Nanoparticles: Assembly, Supramolecular Chemistry, Quantum-Size-Related Properties, and Applications toward Biology, Catalysis, and Nanotechnology. *Chem. Rev.* **2004**, *104*, 293-346.
- 31. Lu, A.-H.; Salabas, E. L.; Schüth, F. Magnetic Nanoparticles: Synthesis, Protection, Functionalization, and Application. *Angew. Chem. Int. Ed.* **2007**, *46*, 1222-1244.
- 32. Zhou, J.; Yang, Y.; Zhang, C-Y. Toward Biocompatible Semiconductor Quantum Dots: From Biosynthesis and Bioconjugation to Biomedical Application. *Chem. Rev.* **2015**, *115*, 11669-11717.
- 33. Chen, Y.; Renner, P.; Liang, H. Dispersion of Nanoparticles in Lubricating Oil: A Critical Review. *Lubricants* **2019**, *7*, 7.
- 34. Ohno, K.; Koh, K.; Tsujii, Y.; Fukuda, T. Fabrication of Ordered Arrays of Gold Nanoparticles Coated with High-Density Polymer Brushes. *Angew. Chem. Int. Ed.* **2003**, *42*, 2751–2754.
- 35. Tang, S. D.; Fox, T. L.; Lo, T.-Y.; Horton, J. M.; Ho, R.-M.; Zhao, B.; Stewart, P. L.; Zhu, L. Environmentally Responsive Self-Assembly of Mixed Poly(tert-butyl acrylate)-Polystyrene Brush-Grafted Silica Nanoparticles in Selective Polymer Matrices. *Soft Matter* **2015**, *11*, 5501-5512.
- 36. Gil, E. S.; Hudson, S. M. Stimuli-Responsive Polymers and their Bioconjugates. *Prog. Polym. Sci.* **2004**, *29*, 1173–1222.
- 37. Roy, D.; Brooks, W. L. A.; Sumerlin, B. S. New Directions in Thermoresponsive Polymers. *Chem Soc. Rev.* **2013**, *42*, 7214-7243.
- 38. Wang, N.; Seymour, B. T.; Lewoczko, E. M.; Kent, E. W.; Chen, M.-L.; Wang, J.-H.; Zhao, B. Zwitterionic Poly(sulfobetaine methacrylate)s in Water: From Upper Critical Solution Temperature (UCST) to Lower Critical Solution Temperature (LCST) with Increasing Length of One Alkyl Substituent on the Nitrogen Atom. *Polym. Chem.* **2018**, *9*, 5257-5261.
- 39. Henn, D. M.; Fu, W. X.; Mei, S.; Li, C. Y.; Zhao, B. Temperature-Induced Shape Changing of Thermosensitive Binary Heterografted Linear Molecular Brushes between Extended Worm-Like and Stable Globular Conformations. *Macromolecules* **2017**, *50*, 1645-1656.
- 40. Bao, C. H.; Horton, J. M.; Bai, Z. F.; Li, D. J.; Lodge, T. P.; Zhao, B. Stimuli-Triggered Phase Transfer of Polymer-Inorganic Hybrid Hairy Particles between Two Immiscible Liquid Phases. *J. Polym. Sci. Part B: Polym. Phys.* **2014**, *52*, 1600-1619.
- 41. Horton, J. M.; Bai, Z. F.; Jiang, X. M.; Li, D. J. Lodge, T. P.; Zhao, B. Spontaneous Phase Transfer of Thermosensitive Hairy Particles between Water and an Ionic Liquid. *Langmuir* **2011**, *27*, 2019-2027.
- 42. Horton, J. M.; Bao, C. H.; Bai, Z. F.; Lodge, T. P.; Zhao, B. Temperature- and pH-Triggered Reversible Transfer of Doubly Responsive Hairy Particles between Water and a Hydrophobic Ionic Liquid. *Langmuir* **2011**, *27*, 13324-13334.

- 43. Wu, T.; Zhang, Y.; Wang, X.; Liu, S. Fabrication of Hybrid Silica Nanoparticles Densely Grafted with Thermoresponsive Poly(*N*-isopropylacrylamide) Brushes of Controlled Thickness via Surface-Initiated Atom Transfer Radical Polymerization. *Chem. Mater.* **2008**, *20*, 101-109.
- 44. Wei, Q.; Ji, J.; Shen, J. Synthesis of Near-Infrared Responsive Gold Nanorod/PNIPAAm Core/Shell Nanohybrids via Surface Initiated ATRP for Smart Drug Delivery. *Macromol. Rapid Commun.* **2008**, *29*, 645–650.
- 45. Tao, H.; Galati, E.; Kumacheva, E. Temperature-Responsive Self-Assembly of Nanoparticles Grafted with UCST Polymer Ligands. *Macromolecules*, **2018**, *51* (15), pp 6021–6027.
- 46. Jiang, X. M.; Wang, B. B.; Li, C. Y.; Zhao, B. Thermosensitive Polymer Brush-Supported 4-*N*,*N*-Dialkylaminopyridine on Silica Particles for Catalysis of Hydrolysis of an Activated Ester in Aqueous Buffers: Comparison of Activity with Linear Polymer-Supported Version and Effect of LCST Transition. *J. Polym. Sci. Part A: Polym. Chem.* **2009**, *47*, 2853-2870.
- 47. Hong, C.-Y.; Li, X.; Pan, C.-Y. Fabrication of smart nanocontainers with a mesoporous core and a pH-responsive shell for controlled uptake and release. *J. Mater. Chem.* **2009**, *19*, 5155-5160.
- 48. Marko, J. F.; Witten, T. A. Phase Separation in a Grafted Polymer Layer. *Phys. Rev. Lett.* **1991**, *66*, 1541–1544.
- 49. Vorselaars, B.; Kim, J. U.; Chantawansri, T. L.; Fredrickson, G. H.; Matsen, M. W. Self-Consistent Field Theory for Diblock Copolymers Grafted to a Sphere. *Soft Matter* **2011**, *7*, 5128-5137.
- 50. Horton, J. M.; Tang, S. D.; Bao, C. H.; Tang, P.; Qiu, F.; Zhu, L.; Zhao, B. Truncated Wedge-Shaped Nanostructures Formed from Lateral Microphase Separation of Mixed Homopolymer Brushes Grafted on 67 nm Silica Nanoparticles: Evidence of the Effect of Substrate Curvature. *ACS Macro Lett.* **2012**, *1*, 1061-1065.
- 51. Chiu, J. J.; Kim, B. J.; Kramer, E. J.; Pine, D. J. Control of Nanoparticle Location in Block Copolymers. *J. Am. Chem. Soc.* **2005**, *127*, 5036–5037.
- 52. Kim, B. J.; Fredrickson, G. H.; Hawker, C. J.; Kramer, E. J. Nanoparticle Surfactants as a Route to Bicontinuous Block Copolymer Morphologies. *Langmuir* **2007**, *23*, 7804–7809.
- 53. Shan, J.; Chen, J.; Nuopponen, M.; Viitala, T.; Jiang, H.; Peltonen, J.; Kauppinen, E.; Tenhu, H. Optical Properties of Thermally Responsive Amphiphilic Gold Nanoparticles Protected with Polymers. *Langmuir* **2006**, *22*, 794–801.
- 54. Zubarev, E. R.; Xu, J.; Sayyad, A.; Gibson, J. D. Amphiphilic Gold Nanoparticles with V-Shaped Arms. *J. Am. Chem. Soc.* **2006**, *128*, 4958–4959.
- 55. Xu, J.; Wang, J.; Mitchell, M.; Mukherjee, P.; Jeffries-El, M.; Petrich, J. W.; Lin, Z. Organic-Inorganic Nanocomposites via Directly Grafting Conjugated Polymers onto Quantum Dots. J. Am. Chem. Soc. 2007, 129, 12828-12833.
- 56. Motornov, M.; Sheparovych, R.; Lupitskyy, R.; MacWilliams, E.; Minko, S. Superhydrophobic Surfaces Generated from Water-Borne Dispersions of Hierarchically Assembled Nanoparticles Coated with a Reversibly Switchable Shell. *Adv. Mater.* **2008**, *20*, 200–205.
- 57. Prucker, O.; Rühe, J. Synthesis of Poly(styrene) Monolayers Attached to High Surface Area Silica Gels through Self-Assembled Monolayers of Azo Initiators. *Macromolecules* **1998**, 31, 592–601.

- 58. Husseman, M.; Malmström, E. E.; McNamara, M.; Mate, M.; Mecerreyes, D.; Benoit, D. G.; Hedrick, J. L.; Mansky, P.; Huang, E.; Russell, T. P.; Hawker, C. J. Controlled Synthesis of Polymer Brushes by "Living" Free Radical Polymerization Techniques. *Macromolecules* **1999**, *32*, 1424-1431.
- 59. Bartholome, C.; Beyou, E.; Bourgeat-Lami, E.; Chaumont, P.; Zydowicz, N. Nitroxide-Mediated Polymerizations from Silica Nanoparticle Surfaces: "Graft from" Polymerization of Styrene Using a Triethoxysilyl-Terminated Alkoxyamine Initiator. *Macromolecules* **2003**, *36*, 7946–7952.
- 60. Yan, J.; Kristufek, T.; Schmitt, M.; Wang, Z.; Xie, G.; Dang, A.; Hui, C. M.; Pietrasik, J.; Bockstaller, M. R.; Matyjaszewski, K. Matrix-free Particle Brush System with Bimodal Molecular Weight Distribution Prepared by SI-ATRP. *Macromolecules* **2015**, 48, 8208–8218.
- 61. Guo, Y.; Moffitt, M. G. Semiconductor Quantum Dots with Environmentally Responsive Mixed Polystyrene/Poly(methyl methacrylate) Brush Layers. *Macromolecules*, **2007**, *40*, 5868–5878.
- 62. Chen, Y.; Yoon, Y. J.; Pang, X.; He, Y.; Jung, J.; Feng, C.; Zhang, G.; Lin, Z. Precisely Size-Tunable Monodisperse Hairy Plasmonic Nanoparticles via Amphiphilic Star-Like Block Copolymers. *Small* **2016**, *12*, 6714-6723.
- 63. Li, D. J.; Sheng, X.; Zhao, B. Environmentally Responsive "Hairy" Nanoparticles: Mixed Homopolymer Brushes on Silica Nanoparticles Synthesized by Living Radical Polymerization Techniques. *J. Am. Chem. Soc.* **2005**, *127*, 6248-6256.
- 64. Zhao, B.; Zhu, L. Nanoscale Phase Separation of Mixed Poly(tert-butyl acrylate)/Polystyrene Brushes on Silica Nanoparticles under Equilibrium Melt Conditions. *J. Am. Chem. Soc.* **2006**, *128*, 4574-4575.
- 65. Zhu, L.; Zhao, B. Transmission Electron Microscopy Study of Solvent-Induced Phase Morphologies of Environmentally Responsive Mixed Homopolymer Brushes on Silica Particles. *J. Phys. Chem. B.* **2008**, *112*, 11529-11536.
- 66. Jiang, X. M.; Zhong, G. J.; Horton, J. M.; Jin, N. X.; Zhu, L.; Zhao, B. Evolution of Phase Morphology of Mixed Poly(tert-butyl acrylate)/Polystyrene Brushes on Silica Particles with the Change of Chain Length Disparity. *Macromolecules* **2010**, *43*, 5387-5395.
- 67. Jiang X. M.; Zhao, B.; Zhong, G. J.; Jin, N. X.; Horton, J. M.; Zhu, L.; Hafner, R. S.; Lodge, T. P. Microphase Separation of High Grafting Density Asymmetric Mixed Homopolymer Brushes on Silica Particles. *Macromolecules* **2010**, *43*, 8209-8217.
- 68. Jiang, B.; Pang, X.; Li, B.; Lin, Z. Organic–Inorganic Nanocomposites via Placing Monodisperse Ferroelectric Nanocrystals in Direct and Permanent Contact with Ferroelectric Polymers. *J. Am. Chem. Soc.* **2015**, *137*, 11760-11767.
- 69. Hiemenz, P. C.; Lodge, T. P. Polymer Chemistry, 2nd ed.; CRC Press: Boca Raton, FL, 2007.
- 70. Wu, C.-S. *Handbook of Size Exclusion Chromatography and Related Techniques*, 2nd ed.; Marcel Dekker: New York, 2004.
- 71. Li, J.; Shiraki, T.; Hu, B.; Wright, R. A. E.; Zhao, B.; Moore, J. S. Mechanophore Activation at Heterointerfaces. *J. Am. Chem. Soc.* **2014**, *136*, 15925–15928.
- 72. Li, J.; Hu, B.; Yang, K.; Zhao, B.; Moore, J. S. Effect of Polymer Grafting Density on Mechanophore Activation at Hereointerfaces. *ACS Macro Lett.* **2016**, *5*, 819-822.
- 73. Ohno, K.; Ma, Y.; Huang, Y.; Mori, C.; Yahata, Y.; Tsujii, Y.; Maschmeyer, T.; Moraes, J.; Perrier, S. Surface-Initiated Reversible Addition-Fragmentation Chain Transfer (RAFT)

- Polymerization from Fine Particles Functionalized with Trithiocarbonates. *Macromolecules* **2011**, *44*, 8944–8953.
- 74. Genzer, J. In Silico Polymerization: Computer Simulation of Controlled Radical Polymerization in Bulk and on Flat Surfaces. *Macromolecules* **2006**, *39*, 7157-7169.
- 75. Turgman-Cohen, S.; Genzer, J. Computer Simulation of Concurrent Bulk- and Surface-Initiated Living Polymerization. *Macromolecules* **2012**, *45*, 2128–2137.
- 76. Matyjaszewski, K.; Xia, J. H. Atom Transfer Radical Polymerization. *Chem. Rev.* **2001**, *101*, 2921–2990.
- 77. Hawker, C. J.; Bosman, A. W.; Harth, E. New Polymer Synthesis by Nitroxide Mediated Living Radical Polymerizations. *Chem. Rev.* **2001**, *101*, 3661–3688.
- 78. Moad, G.; Rizzardo, E.; Thang, S. H. Toward Living Radical Polymerization. *Acc. Chem. Res.* **2008**, *41*, 1133–1142.
- 79. Hu, B.; Henn, D. M.; Wright, R. A. E.; Zhao, B. Hybrid Micellar Hydrogels of a Thermosensitive ABA Triblock Copolymer and Hairy Nanoparticles: Effect of Spatial Location of Hairy Nanoparticles on Gel Properties. *Langmuir* **2014**, *30*, 11212-11224.
- 80. Hu, B.; Fu, W. X.; Zhao, B. Enhancing Gelation of Thermosensitive Hydrophilic ABC Linear Triblock Copolymers in Water by Thermoresponsive Hairy Nanoparticles. *Macromolecules* **2016**, *49*, 5502-5513.
- 81. Li, W.; Bao, C. H.; Wright, R. A. E.; Zhao, B. Synthesis of Mixed Poly(ε-caprolactone)/Polystyrene Brushes from Y-Initiator-Functionalized Silica Particles by Surface-Initiated Ring-Opening Polymerization and Nitroxide-Mediated Radical Polymerization. *RSC Adv.* **2014**, *4*, 18772-18781.
- 82. Wang, B. B.; Li, B.; Dong, B.; Zhao, B.; Li, C. Y. Homo- and Hetero-Particle Clusters Formed by Janus Nanoparticles with Bicompartment Polymer Brushes. *Macromolecules* **2010**, *43*, 9234-9238.
- 83. Wang, B. B.; Dong, B.; Li, B.; Zhao, B.; Li, C. Y. Janus Gold Nanoparticle with Bicompartment Polymer Brushes Templated by Polymer Single Crystals. *Polymer* **2010**, *51*, 4814-4822.
- 84. Halperin, A.; Tirrell, M.; Lodge, T. P. Tethered Chains in Polymer Microstructures. *Adv. Polym. Sci.* **1992**, *100*, 31–71.
- 85. Tsujii, Y.; Ohno, K.; Yamamoto, S.; Goto, A.; Fukuda, T. Structure and Properties of High-Density Polymer Brushes Prepared by Surface-Initiated Living Radical Polymerization. *Adv. Polym. Sci.* **2006**, *197*, 1–45.
- 86. Chen, W. Y.; Zheng, J. X.; Cheng, S. Z. D.; Li, C. Y.; Huang, P.; Zhu, L.; Xiong, H.; Ge, Q.; Guo, Y.; Quirk, R. P.; Lotz, B.; Deng, L.; Wu, C.; Thomas, E. L. Onset of Tethered Chain Overcrowding. *Phys. Rev. Lett.* **2004**, *93*, 028301.
- 87. Zheng, J. X.; Xiong, H. M.; Chen, W. Y.; Lee, K.; Van Horn, R. M.; Quirk, R. P.; Lotz, B.; Thomas, E. L.; Shi, A.-C.; Cheng, S. Z. D. Onsets of Tethered Chain Overcrowding and Highly Stretched Brush Regime via Crystalline–Amorphous Diblock Copolymers. *Macromolecules* **2006**, *39*, 641–650.
- 88. Choi, J.; Dong, H.; Matyjaszewski, K.; Bockstaller, M. R. Flexible Particle Array Structures by Controlling Polymer Graft Architecture. *J. Am. Chem. Soc.* **2010**, *132*, 12537-12539.
- 89. Ohno, K.; Morinaga, T.; Takeno, S.; Tsujii, Y.; Fukuda, T. Suspensions of Silica Particles Grafted with Concentrated Polymer Brush: Effects of Graft Chain Length on Brush Layer Thickness and Colloidal Crystallization. *Macromolecules*, **2007**, *40*, 9143–9150.

- 90. Daoud, M.; Cotton, J. P. Star Shaped Polymers: A Model for the Conformation and its Concentration Dependence. *J. Phys. (Paris)* **1982**, *43*, 531–538.
- 91. Choi, J.; Hui, C. M.; Pietrasik, J.; Dong, H.; Matyjaszewski, K.; Bockstaller, M. R. Toughening Fragile Matter: Mechanical Properties of Particle Solids Assembled from Polymer-Grafted Hybrid Particles Synthesized by ATRP. *Soft Matter* **2012**, *8*, 4072-4082.
- 92. Williams, D. B.; Carter, C. B. *Transmission Electron Microscopy: A Textbook for Materials Science*, 2nd ed.; Springer: Boston, MA, 2009.
- 93. Lin, Y.-S., Hurley, K. R., and Haynes, C.L. Critical Considerations in the Biomedical Use of Mesoporous Silica Nanoparticles. *J. Phys. Chem. Lett.* **2012**, *3*, 364-374.
- 94. Zhang, J.; Chai, S.-H.; Qiao, Z.-A.; Mahurin, S. M.; Chen, J.; Fang, Y.; Wan, S.; Nelson, K.; Zhang, P.; Dai, S. Porous Liquids: A Promising Class of Media for Gas Separation. *Angew. Chem. Int. Ed.* **2015**, *54*, 932-936.
- 95. Möller, K.; Bein, T. Talented Mesoporous Silica Nanoparticles. *Chem. Mater.* **2017**, *29*, 371-388.
- 96. Blas, H.; Save, M.; Boissière, C.; Sanchez, C.; Charleux, B. Surface-Initiated Nitroxide-Mediated Polymerization from Ordered Mesoporous Silica. *Macromolecules* **2011**, *44*, 2577-2588.
- 97. Lowell, S.; Shields, J. E.; Thomas, M. A.; Thommes, M. In Characterization of Porous Solids and Powders: Surface Area, Pore Size and Density; Lowell, S.; Shields, J. E.; Thomas, M. A.; Thommes, M., Ed.; Springer: Dordrecht, 2004; pp 58-81.
- 98. Hamley, I. W. *Introduction to Soft Matter: Polymers, Colloids Amphiphiles, and Liquid Crystals*, 1st ed.; Wiley: New York, 2000.
- 99. Seymour, B. T.; Wright, R. A. E.; Parrott, A. C.; Gao, H. Y.; Martini, A.; Qu, J.; Dai, S.; Zhao, B. Poly(alkyl methacrylate) Brush-Grafted Silica Nanoparticles as Oil Lubricant Additives: Effects of Alkyl Pendant Groups on Oil Dispersibility, Stability, and Lubrication Property. *ACS Appl. Mater. Interfaces*, **2017**, *9*, 25038–25048.
- 100. Seymour, B. T.; Fu, W.; Wright, R. A. E.; Luo, H.; Qu, J.; Dai, S.; Zhao, B. Improved Lubricating Performance by Combining Oil-Soluble Hairy Silica Nanoparticles and an Ionic Liquid as an Additive for a Synthetic Base Oil. *ACS Appl. Mater. Interfaces* **2018**, *10*, 15129–15139.
- 101. Shan, J.; Chen, J.; Nuopponen, M.; Tenhu, H. Two Phase Transitions of Poly(N-isopropylacrylamide) Brushes Bound to Gold Nanoparticles. *Langmuir* **2004**, *20*, 4671-4676.
- 102. Chen, C.; Zhang, T.; Zhu, L.; Zhao, B.; Tang, P.; Qiu, F. Hierarchical Superstructures Assembled by Binary Hairy Nanoparticles. *ACS Macro Lett.* **2016**, *5*, 718-723.
- 103. Guzman-Juarez, B.; Abdelaal, A.; Kim, K.; Toader, V.; Reven, L. Fabrication of Amphiphilic Nanoparticles via Mixed Homopolymer Brushes and NMR Characterization of Surface Phase Separation. *Macromolecules* **2018**, *51*, 9951-9960.
- 104. Motornov, M.; Sheparovych, R.; Lupitskyy, R.; MacWilliams, E.; Minko, S. Responsive Colloidal Systems: Reversible Aggregation and Fabrication of Superhydrophobic Surfaces. *J. Colloid Interface Sci.* **2007**, *310*, 481–488.
- 105. Egerton, R. F. *Physical Principles of Electron Microscopy: An Introduction to TEM, SEM, and AEM*, 2nd ed.; Springer: Switzerland, 2016.
- 106. Ercius, P.; Alaidi, O.; Rames, M. J.; Ren, G. Electron Tomography: A Three-Dimensional Analytic Tool for Hard and Soft Materials Research. *Adv. Mater.* **2015**, *27*, 5638-5663.
- 107. Midgley, P. A.; Dunin-Borkowski, R. E. Electron Tomography and Holography in Materials Science. *Nat. Mater.* **2009**, *8*, 271-280.

- 108. Tang, S. D.; Lo, T.-Y.; Horton, J. M.; Bao, C. H.; Tang, P.; Qiu, F.; Ho, R.-M.; Zhao, B.; Zhu, L. Direct Visualization of Three-Dimensional Morphology in a Dense Monolayer Film of Mixed Poly(*tert*-Butyl Acrylate)/Polystyrene Brush-Grafted Silica Nanoparticles. *Macromolecules* **2013**, *46*, 6575-6584.
- 109. Fox, T. L.; Tang, S. D.; Horton, J. M.; Holdaway, H. A.; Zhao, B.; Zhu, L.; Stewart, P. L. In Situ Characterization of Binary Mixed Polymer Brush-Grafted Silica Nanoparticles in Aqueous and Organic Solvents by Cryo-Electron Tomography. *Langmuir* **2015**, *31*, 8680-8688.
- 110. Green, P. F. The Structure of Chain End-Grafted Nanoarticle/Homopolymer Nanocomposites. *Soft Matter* **2011**, *7*, 7914.
- 111. Schaefer, D. W.; Justice, R. S. How Nano are Nanocomposites. *Macromolecules* **2007**, *40*, 8501–8517.
- 112. Chevigny, C.; Jestin, J.; Gigmes, D.; Schweins, R.; Di-Cola, E.; Dalmas, F.; Bertin, B.; Boué, F. "Wet-to-Dry" Conformational Transition of Polymer Layers Grafted to Nanoparticles in Nanocomposite. *Macromolecules* **2010**, *43*, 4833–4837.
- 113. He, J.; Liu, Y.; Babu, T.; Wei, Z.; Nie, Z. Self-Assembly of Inorganic Nanoparticle Vesicles and Tubules Driven by Tethered Linear Block Copolymers. *J. Am. Chem. Soc.* **2012**, *134*, 11342-11345.
- 114. Stewart, P. L. Cryo-Electron Microscopy and Cryo-Electron Tomography of Nanoparticles. *WIREs Nanomed. Nanobiotechnol.* **2016**, *9*, e1417.

# **Table of Contents Graphic:**

